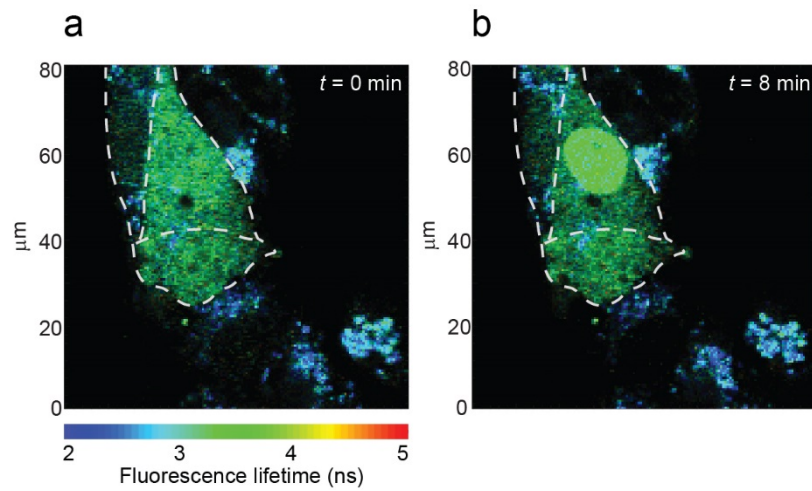


**Supplementary Figure 1**

Testing cell integrity after microinjection.

(a) HeLa cells before injection at pH 7.2, in HBSS buffer. Cells that were to be injected are indicated by a yellow dot. (b) The same cells 15 min after microinjection of 20 mM sodium phosphate buffer (0.5 bar, 50 ms pulse duration, one injection per cell); only minor morphological changes of the injected cells are visible. (c) 40 min after injection; an overlay of a phase contrast image and the fluorescence image after addition of propidium iodide to the culture medium shows no signs of cell blebbing or cell death of the injected cells. The three red fluorescent spots originate from dead cells already present before injection. (d) 1.5 h after injection; four cells (18% of injected cells) formed blebs (indicated by blue arrows), and one dead cell is visible upon propidium iodide staining.



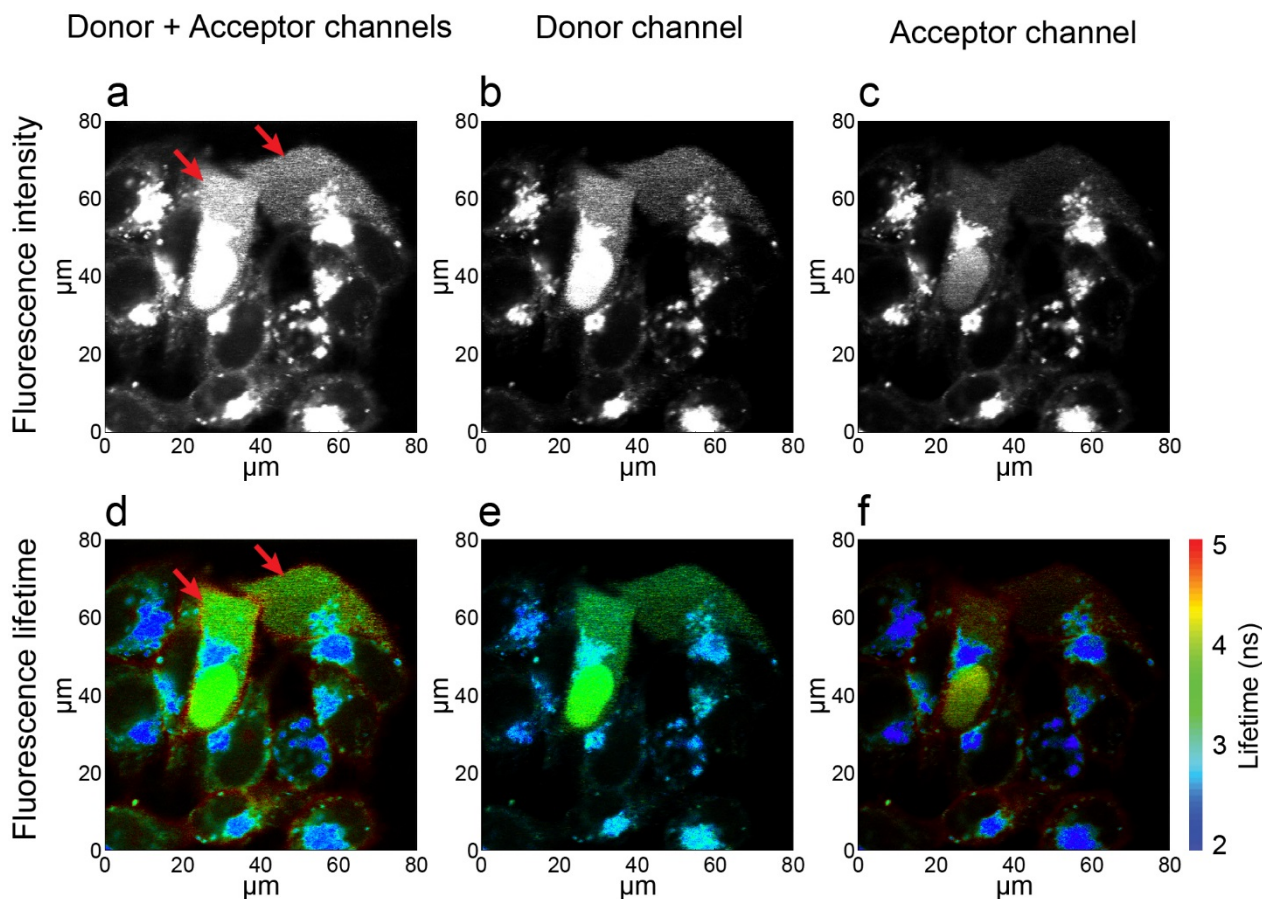
## Supplementary Figure 2

Nuclear localization of ProT $\alpha$  observed after microinjection.

(a) FLIM image showing the uniform distribution of ProT $\alpha$  directly after injection of ProT $\alpha$  into the cytosol of three different HeLa cells (cell boundaries indicated by dashed lines). Due to differences in injection efficiency, the ProT $\alpha$  concentration in the left cell is slightly lower than in the other two cells. (b) 8 min later, an accumulation of ProT $\alpha$  in the nucleus of the middle cell is visible, indicating active nuclear transport<sup>1</sup>. The absence of nuclear accumulation in some cells may be due to cell cycle differences<sup>2</sup>.

### References:

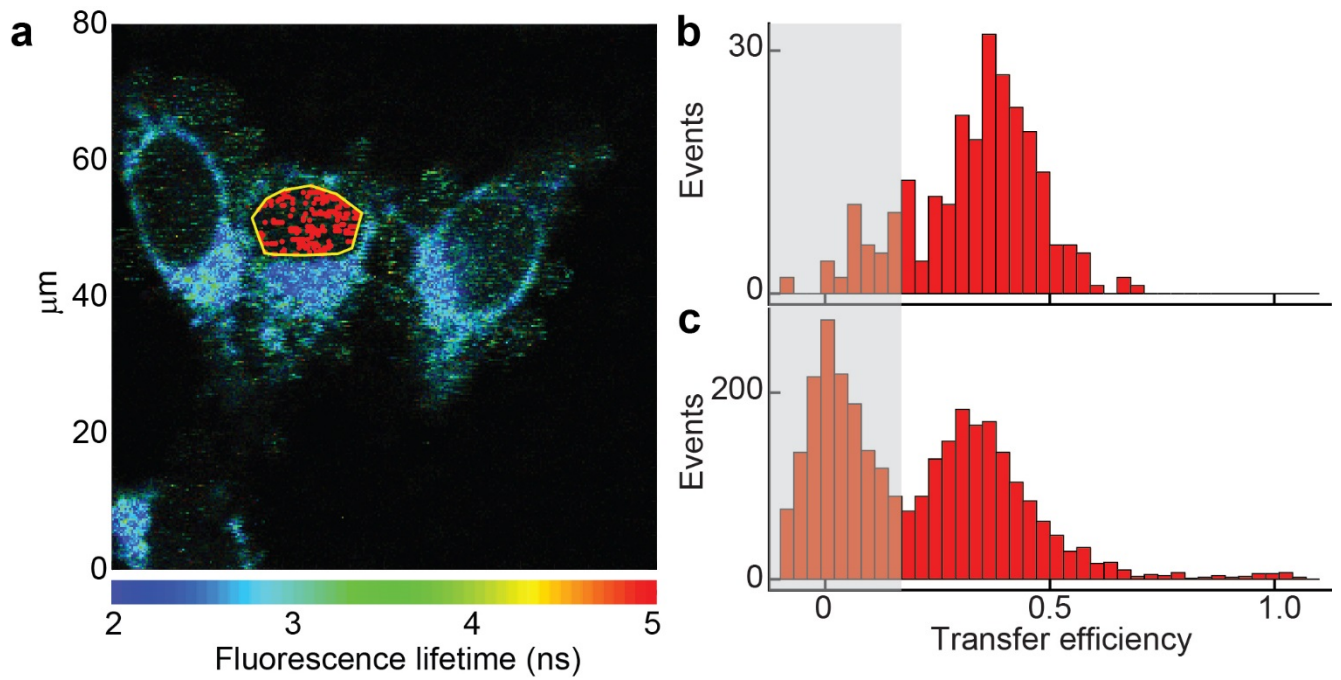
1. Manrow, R.E., Sburlati, A.R., Hanover, J.A. & Berger, S.L. Nuclear targeting of prothymosin alpha. *J. Biol. Chem.* **266**, 3916-3924 (1991).
2. Martin-Aparicio, E., Avila, J. & Lucas, J.J. Nuclear localization of N-terminal mutant huntingtin is cell cycle dependent. *Eur. J. Neurosci.* **16**, 355-359 (2002).



### Supplementary Figure 3

Comparison of fluorescence intensity and fluorescence lifetime images.

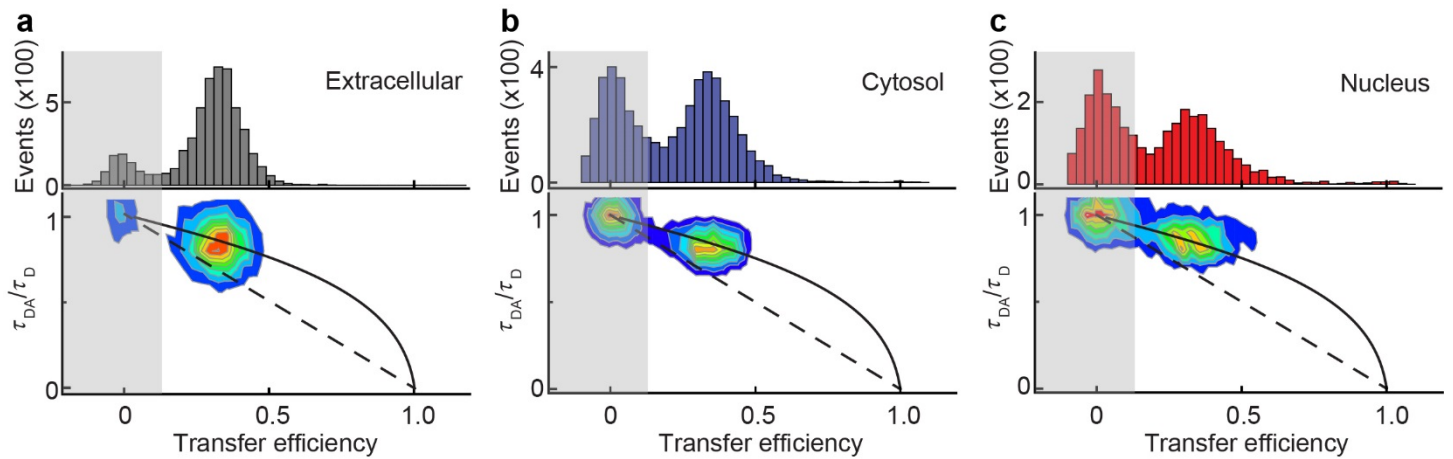
This array of images compares fluorescence intensity and lifetime images of HeLa cells. The same scan is shown in **Figure 1b**, where two cells were injected with fluorescently labeled ProTα (red arrows in **(a)** and **(d)**). The upper row shows only fluorescence intensities, with **(a)** showing donor and acceptor channels combined, **(b)** only the donor channel, and **(c)** only the acceptor channel. The lower row additionally uses the fluorescence lifetime information, with **(d)** donor and acceptor channels combined, **(e)** only the donor channel, and **(f)** only the acceptor channel (color code to the right). The comparison illustrates that fluorescence intensity information is sufficient to distinguish injected from non-injected cells, but lifetime information can be helpful additionally, e.g. to aid the distinction of fluorescence from injected sample and cellular autofluorescence (if differences in lifetimes exist).



#### Supplementary Figure 4

Extracting FRET efficiency histograms of intracellular ProT $\alpha$  from area scans.

To clarify whether an immobile subpopulation with different conformational properties from freely diffusing molecules was present, the confocal volume was scanned over an area of 80 by 80  $\mu\text{m}$  in the cell during data acquisition. **(a)** Area scan showing HeLa cells after injection of FRET-labeled ProT $\alpha$  in the cytosol. The image was recorded with a resolution of 256 x 256 pixels and a scanning speed of 0.5 pixel/ms. The color of each pixel indicates the fluorescence lifetime. The yellow polygon indicates the area (nucleus of the middle cell) where burst detection was carried out. The red dots within the polygon indicate the positions of photon bursts detected during scanning, which were used to construct the FRET efficiency histogram in **(b)**. **(b)** FRET efficiency histogram of ProT $\alpha$  constructed from the FLIM image. The average transfer efficiency determined from area scans in the nuclei of three different cells was  $0.34 \pm 0.03$ . The population at zero transfer efficiency (shaded) originates from molecules lacking active acceptor chromophores. **(c)** The sum of all transfer efficiency histograms of ProT $\alpha$  measured in the nucleus of HeLa cells without scanning shows a transfer efficiency of  $0.35 \pm 0.03$ , indicating the absence of immobile ProT $\alpha$  with a transfer efficiency different from freely diffusing molecules. Note also that the lower number of events with a transfer efficiency close to zero in **(b)** compared to **(c)** indicates a pronounced contribution of photobleaching to the donor-only population.



### Supplementary Figure 5

Fluorescence lifetime vs. transfer efficiency histograms of ProT $\alpha$ .

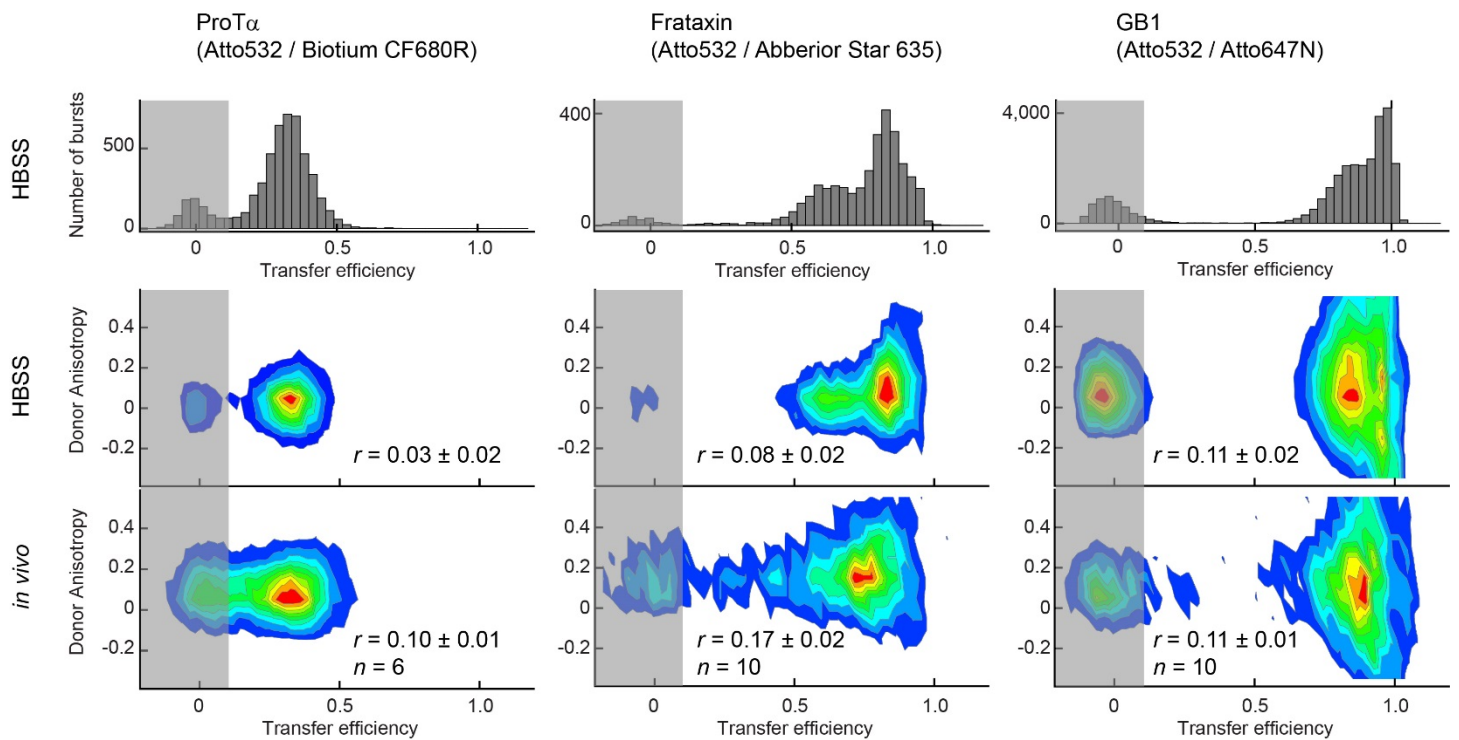
Transfer efficiency histograms (top) and the corresponding two-dimensional histograms of relative donor fluorescence lifetime ( $\tau_{DA}/\tau_D$ , where  $\tau_{DA}$  is the lifetime in the presence and  $\tau_D$  in the absence of acceptor) versus transfer efficiency (bottom) of ProT $\alpha$  (a) in the extracellular medium; (b) the sum of all histograms measured in the cytosol ( $n = 8$ ); and (c) in the nucleus ( $n = 8$ ) of HeLa cells incubated in a cell culture medium with  $I = 156$  mM. The dashed line shows the expected relation between the average values of  $\tau_{DA}/\tau_D$  and transfer efficiency for a fixed distance between the two fluorophores, the solid line the relation for a chain sampling a broad distribution of distances corresponding to a Gaussian chain<sup>3</sup> (Online Methods). The population of unfolded ProT $\alpha$  is close to the solid line in all three cases, indicating that ProT $\alpha$  is rapidly reconfiguring not only in buffer<sup>3</sup> but also within the cells. The peaks at zero transfer efficiency (shaded) are due to molecules lacking an active acceptor dye and serve as a reference for determining  $\tau_D$ .

Note that the peak at zero transfer efficiency is larger for intracellular (b,c) compared with the extracellular measurement (a), but the contribution of intracellular background to the “donor-only” peak is small, as indicated by measurements in non-injected cells (Supplementary Fig. 14) and in agreement with the high yields of doubly-labeled protein (Online Methods). Additionally, the absolute fluorescence lifetime of this “donor-only” population is not significantly different from the donor lifetime in extracellular measurements (3.8 ns in extracellular medium, 3.8 ns in the cytosol, and 3.9 ns in the nucleus) and is thus most likely to be due to a preferential inactivation of the acceptor dye by photobleaching (see also Supplementary Fig. 4) or to cellular degradation of part of the injected molecules.

We note that it will be interesting to investigate variations in biomolecular conformation or folding mechanism by positioning the observation volume in different regions within the cell or on the plasma membrane (within the spatial resolution of the diffraction-limited confocal volume), e.g. for DNA-binding proteins that fold upon binding their target in the nucleus, or for membrane proteins, respectively.

References:

3. Soranno, A. et al. Quantifying internal friction in unfolded and intrinsically disordered proteins with single molecule spectroscopy. *Proc. Natl. Acad. Sci. USA* **109**, 17800-17806 (2012).



### Supplementary Figure 6

Comparison of donor fluorescence anisotropies from confocal single-molecule measurements *in vitro* and *in vivo*.

Donor fluorescence anisotropies for ProTα (labeled with Atto 532/Biotium CF680R), frataxin (Atto 532/Abberior Star 635), and GB1 (Atto 532/Atto 647N) upon excitation at 520 nm from confocal single-molecule measurements *in vitro* (in HBSS, histograms and first row of donor anisotropy vs. transfer efficiency plots) and in HeLa cells (*in vivo*, bottom row). The areas shaded in gray indicate the donor-only population and were not used for the analysis of the donor anisotropy. The donor anisotropies,  $r$ , were calculated for every fluorescence burst with a transfer efficiency greater than 0.2 using<sup>4-6</sup>

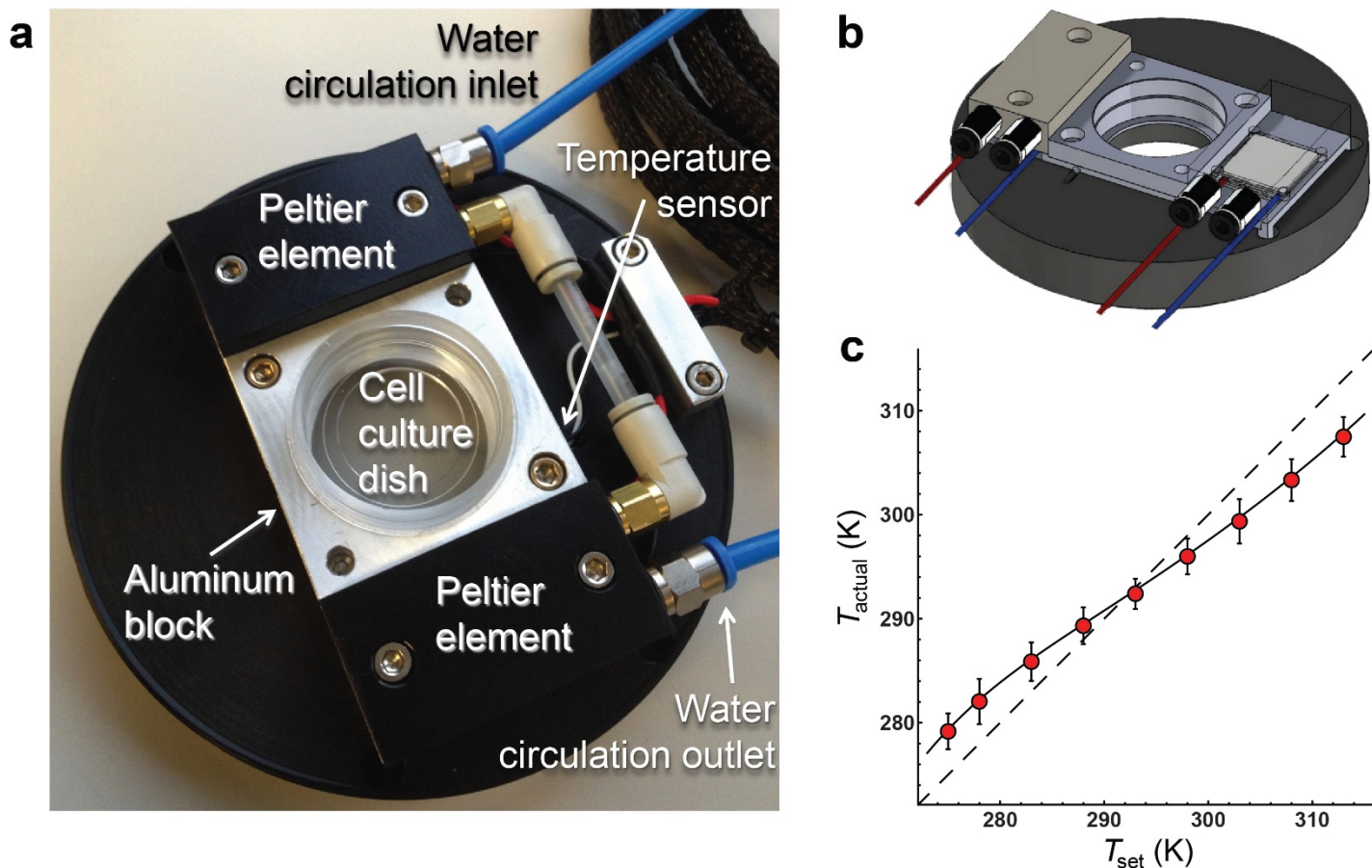
$$r = \frac{n_p - G \cdot n_s}{(1 - 3L_2)n_p + (2 - 3L_1)G \cdot n_s}$$

where  $n_{p,s}$  are the numbers of donor photons in a burst with parallel ( $p$ ) and perpendicular polarization ( $s$ ) with respect to the polarization of the excitation light;  $G$  is a correction factor for differences in detection efficiencies in the parallel and the perpendicular donor channels ( $G_{\text{Atto532/CF680R}} = 1.08$ ,  $G_{\text{Atto532/AS635}} = 1.11$ ,  $G_{\text{Atto532/Atto647N}} = 1.11$ ), and  $L_{1,2}$  are factors correcting primarily for the effect of the high numerical aperture lens used for excitation and detection<sup>4,5</sup> ( $L_1 = 0.098$ ,  $L_2 = 0.094$ )<sup>6</sup>. Mean anisotropies were calculated by combining all photons from bursts with  $E > 0.2$  and calculating  $r$  as shown above.

Donor fluorescence anisotropies in buffer were found to be  $0.03 \pm 0.02$  for ProTα,  $0.08 \pm 0.02$  for frataxin, and  $0.11 \pm 0.02$  for GB1. The uncertainties in the values in buffer were estimated by error propagation assuming an uncertainty in  $G$  of 5%. Anisotropies *in vivo* were higher than in buffer for ProTα ( $0.10 \pm 0.01$ , mean and standard deviation from 6 cells) and frataxin ( $0.17 \pm 0.02$ , mean and standard deviation from 10 cells). In the case of GB1, the anisotropy *in vivo* ( $0.11 \pm 0.01$ , mean and standard deviation from 10 cells) was not significantly higher than *in vitro*.

#### References:

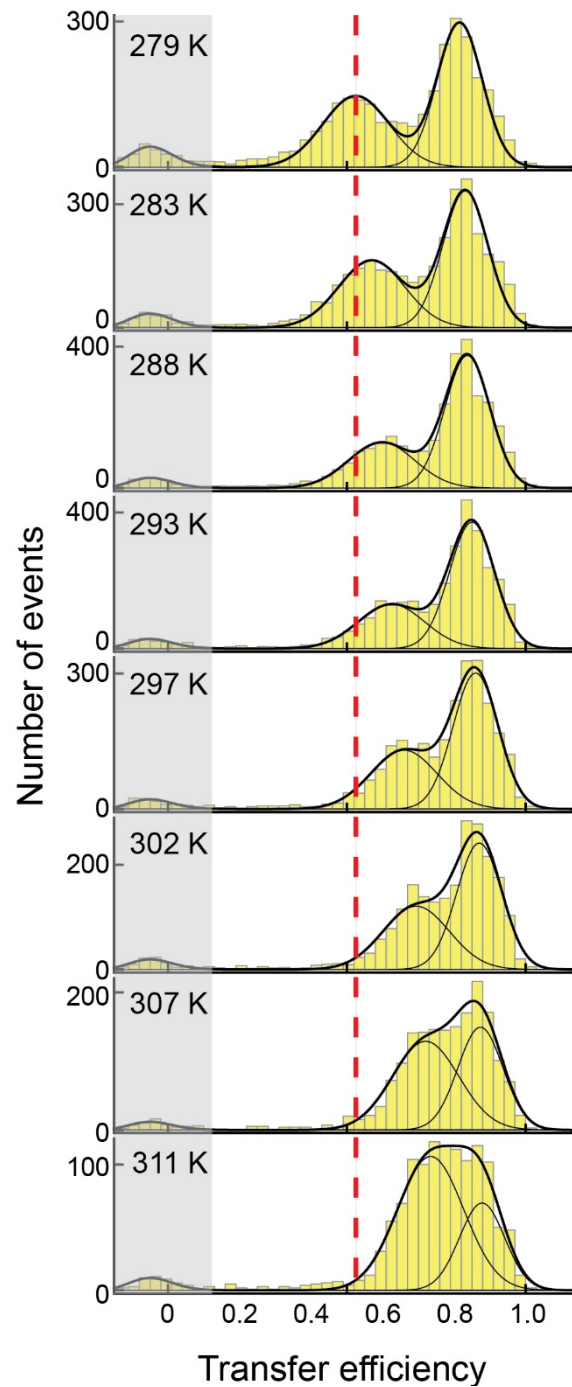
- Koshioka, M., Sasaki, K. & Masuhara, H. Time-Dependent Fluorescence Depolarization Analysis in 3-Dimensional Microspectroscopy. *Appl. Spectrosc.* **49**, 224-228 (1995).
- Schaffer, J. et al. Identification of single molecules in aqueous solution by time-resolved fluorescence anisotropy. *J Phys Chem A* **103**, 331-336 (1999).
- Kellner, R. et al. Single-molecule spectroscopy reveals chaperone-mediated expansion of substrate protein. *Proc. Natl. Acad. Sci. USA* **111**, 13355-13360 (2014).



**Supplementary Figure 7**

Custom-built temperature-controlled holder for cell culture dishes.

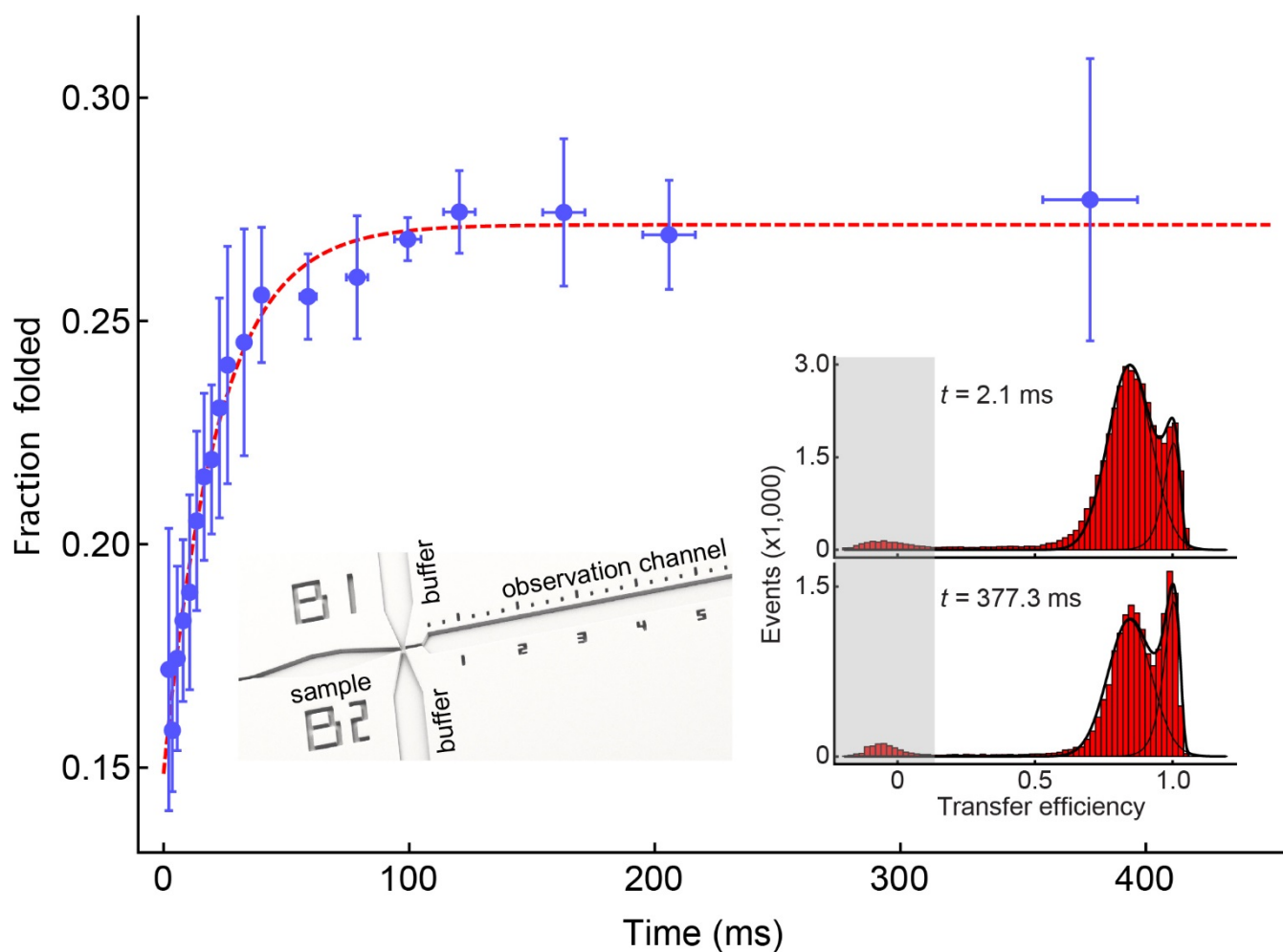
(a) Photograph of the temperature-controlled cell culture dish holder for the intracellular single-molecule FRET experiments. (b) Schematic drawing of the holder. (c) Temperature calibration based on the temperature-dependent fluorescence lifetime measurements of rhodamine B shows the conversion of the value measured at the sensor in the aluminum block to the actual temperature in the confocal volume. Error bars reflect the uncertainty in the fluorescence lifetime measurements used for calibration.



### Supplementary Figure 8

FRET histograms of Yff1 in HBSS as a function of temperature.

FRET histograms of Yff1 in HBSS as a function of temperature showing the heat and cold denaturation and the temperature-induced collapse of unfolded Yff1 *in vitro*. The dashed red line indicates the position of unfolded Yff1 at 279 K. The peak at  $E \approx 0.85$  corresponds to the folded population, the peak at lower transfer efficiencies to the unfolded population of Yff1. The peak close to a transfer efficiency of zero (shaded) corresponds to a population of molecules lacking an active acceptor chromophore. Solid lines are fits with two Gaussian peak functions (for details of the fitting procedure, see Online Methods) corresponding to unfolded and folded subpopulations (sum shown as thick solid line).



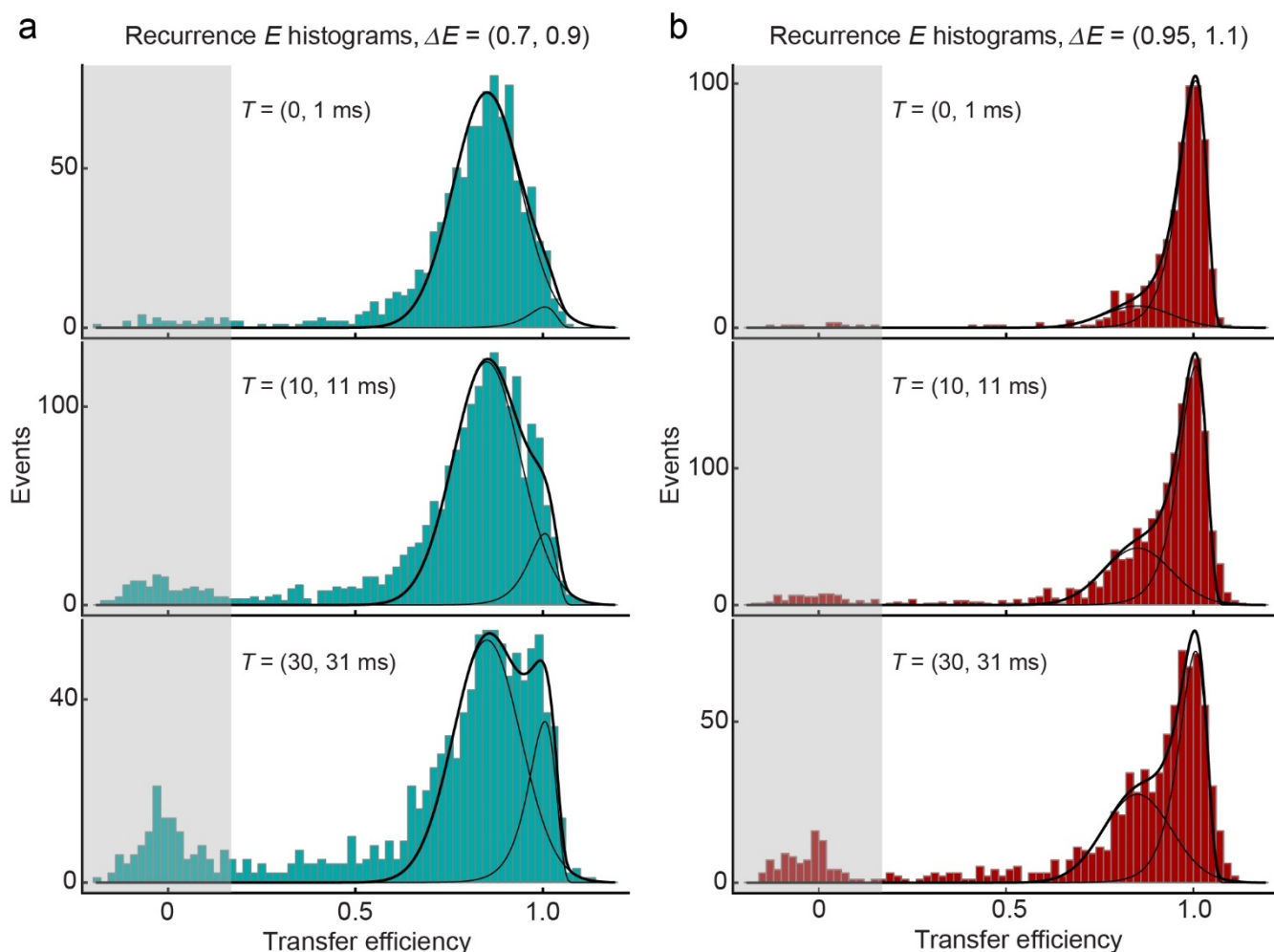
### Supplementary Figure 9

Microfluidic mixing experiment of the folding of GB1 in buffer.

Microfluidic mixing experiment showing the folding of GB1 after rapid dilution of GB1 in 0.8 M GdmCl to 80 mM GdmCl at 4 °C. The error bars along the time axis describe the uncertainty originating from the positioning of the confocal volume along the observation channel and the uncertainty in flow velocity. For the uncertainty in the arrival time, we assumed a variation in the flow velocity of 5% and an uncertainty of 0.5  $\mu\text{m}$  in positioning the laser focus<sup>7</sup>. The error bars in ordinate direction indicate the standard deviation of the fraction folded from the FRET efficiency histograms of three individual measurements. The insets show an electron microscopy image of the microfluidic mixing chamber with the observation channel, the two buffer inlets and the sample inlet channel (left), and representative FRET efficiency histograms measured after 2.1 ms and 377 ms, respectively (right). The peak close to a transfer efficiency of zero (shaded) corresponds to a population of molecules lacking an active acceptor chromophore. The fraction of unfolded GB1 ( $\langle E \rangle = 0.85$ ) decreases over time and the fraction of folded GB1 ( $\langle E \rangle = 1.00$ ) increases.

References:

7. Wunderlich, B. et al. Microfluidic mixer designed for performing single-molecule kinetics with confocal detection on timescales from milliseconds to minutes. *Nat. Protoc.* **8**, 1459-1474 (2013).



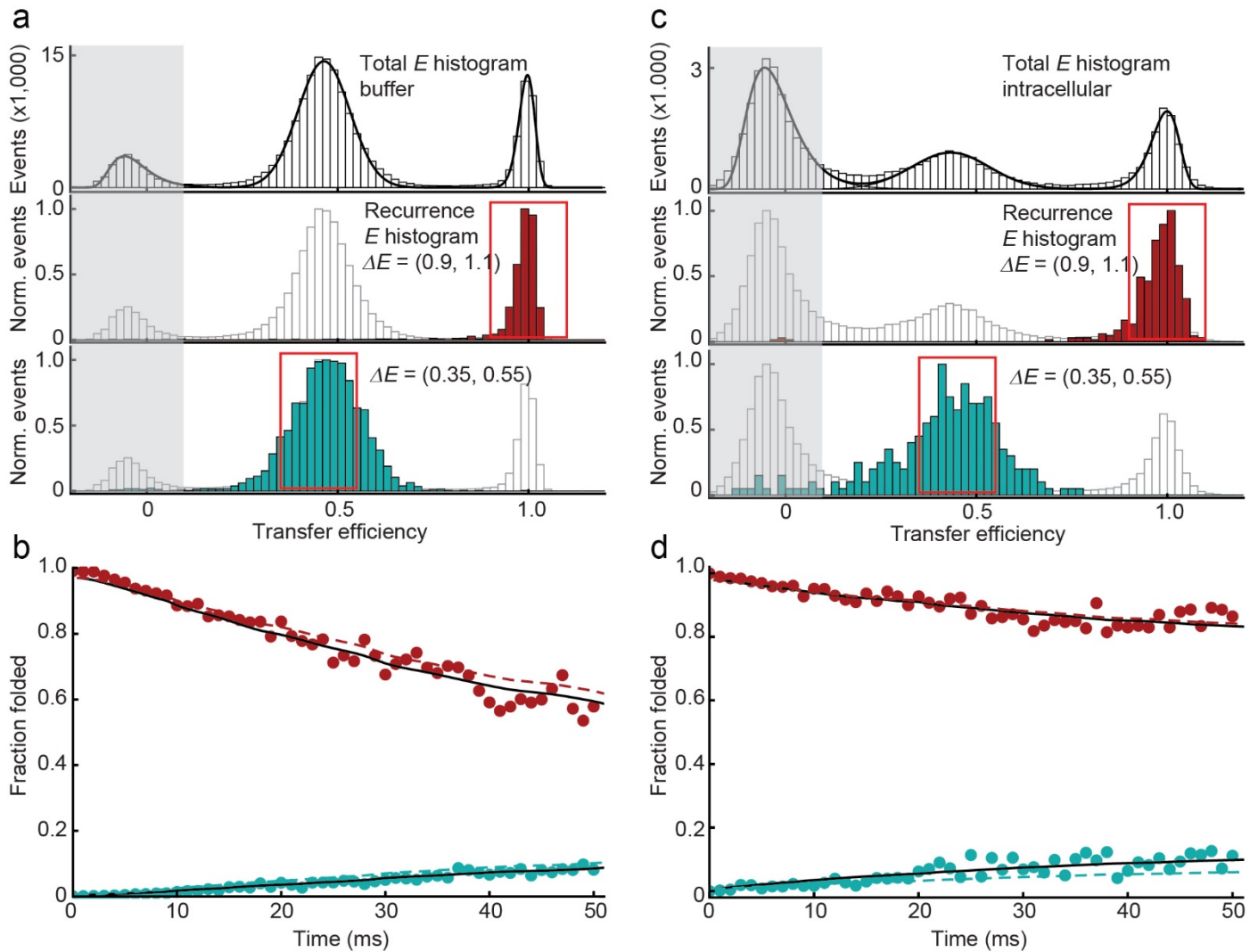
### Supplementary Figure 10

Recurrence transfer efficiency histograms of GB1 in HeLa cells.

(a) Recurrence transfer efficiency histograms<sup>8</sup> of GB1 measured intracellularly with an initial transfer efficiency range  $\Delta E$  of 0.7 – 0.9 (corresponding to the unfolded state), showing the depopulation of unfolded GB1 with increasing recurrence intervals,  $T$ . Starting from the unfolded state, the increase in the folded-state population at  $\langle E \rangle = 1.00$  originates from the increase in the probability of observing a folded molecule with increasing time between the first and second observed fluorescence burst due to the folding/unfolding dynamics. The peak close to a transfer efficiency of zero (shaded) corresponds to a population of molecules lacking an active acceptor chromophore. (b) The conversion of folded to unfolded GB1 is shown in the recurrence histograms with an initial transfer efficiency range  $\Delta E$  of 0.95 – 1.1 (corresponding to the folded state). Starting from the folded state, the increase in the unfolded-state population at lower transfer efficiency originates from the increase in the probability of observing an unfolded molecule with increasing time between the first and second observed fluorescence burst due to the folding/unfolding dynamics. A global analysis of 61 histograms of this type was used for the kinetics shown in **Figure 4**.

References:

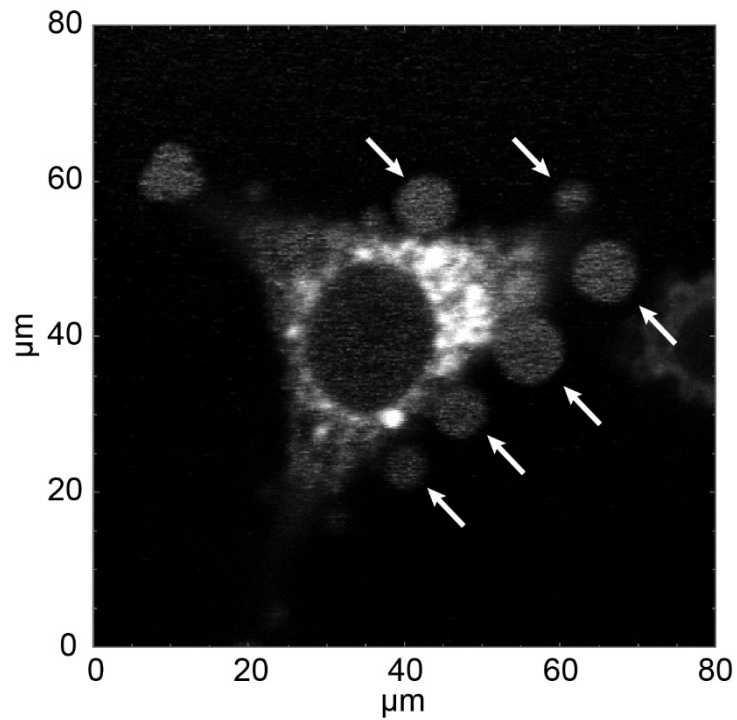
- Hoffmann, A. et al. Quantifying heterogeneity and conformational dynamics from single molecule FRET of diffusing molecules: recurrence analysis of single particles (RASP). *Phys. Chem. Chem. Phys.* **13**, 1857-1871 (2011).



**Supplementary Figure 11**

RASP control measurement with a noninterconverting mixture of ProT $\alpha$  and GB1 wild type (wt).

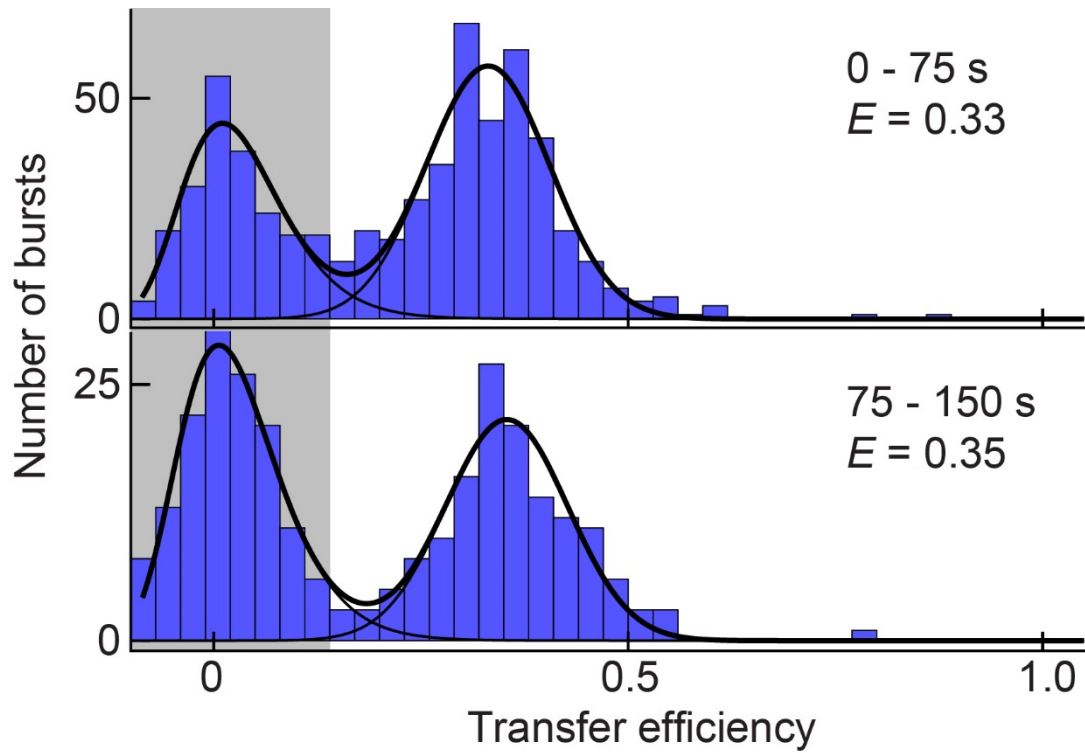
To illustrate the results from RASP<sup>6</sup> for two species that do not interconvert, a mixture of FRET-labeled ProT $\alpha$  and GB1 wt were co-injected into HeLa cells. **(a)** FRET efficiency histogram of a mixture of 20 pM ProT $\alpha$  and 20 pM GB1 wt in HBSS, pH 7.2, measured for 15 h at 4 °C, with recurrence histograms of GB1 wt (red, initial  $E$  range  $\Delta E = (0.9 - 1.1)$ ) and ProT $\alpha$  (cyan, initial  $E$  range  $\Delta E = (0.35 - 0.55)$ ), both within a recurrence interval of  $T = (0, 1)$  ms). The peak close to a transfer efficiency of zero (shaded) corresponds to a population of molecules lacking an active acceptor chromophore. **(b)** Recurrence analysis indicates that changes in the fraction of folded molecules with increasing delay times are only due to the occurrence of “new” (i.e. non-recurring) molecules, as shown by the coincidence between a global fit of the data with a model<sup>6</sup> including both folding and unfolding of recurring molecules and the appearance of new molecules (solid line) and the changes expected from the arrival of new molecules alone (dashed lines). **(c)** The same behavior was found with GB1 wt and ProT $\alpha$  injected into HeLa cells (red and cyan, respectively, with the same initial  $E$  ranges as in **(a)**). The total  $E$  histogram was constructed from measurements in 51 individual cells with a total measurement time of 2.8 h. **(d)** Similar to the finding in buffer, no interconversion between the two populations was observed but only changes due to the arrival of new molecules.



#### Supplementary Figure 12

Example of a HeLa cell showing membrane protuberances after microinjection.

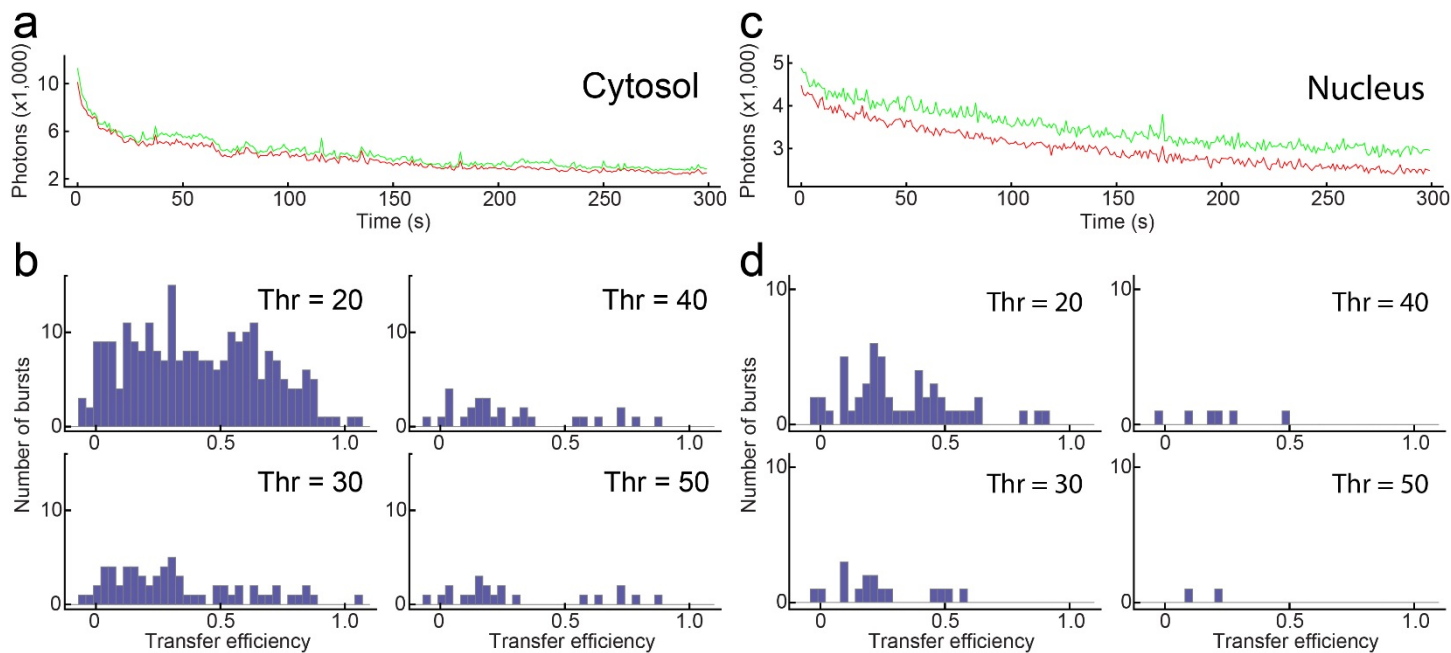
Fluorescence intensity scan of a HeLa cell microinjected using too high a pressure. One injection with a pressure of 1 bar and a pulse duration of 50 ms was applied to inject a solution of fluorescently labeled ProTα. The formation of membrane protuberances after injection (indicated with white arrows) clearly indicates that the applied pressure was too high or the pulse duration too long. Injection settings were chosen in order that the formation of such protuberances did not occur but sufficient fluorescently labeled sample was injected.



**Supplementary Figure 13**

Change of the FRET efficiency distribution during a measurement in a single cell.

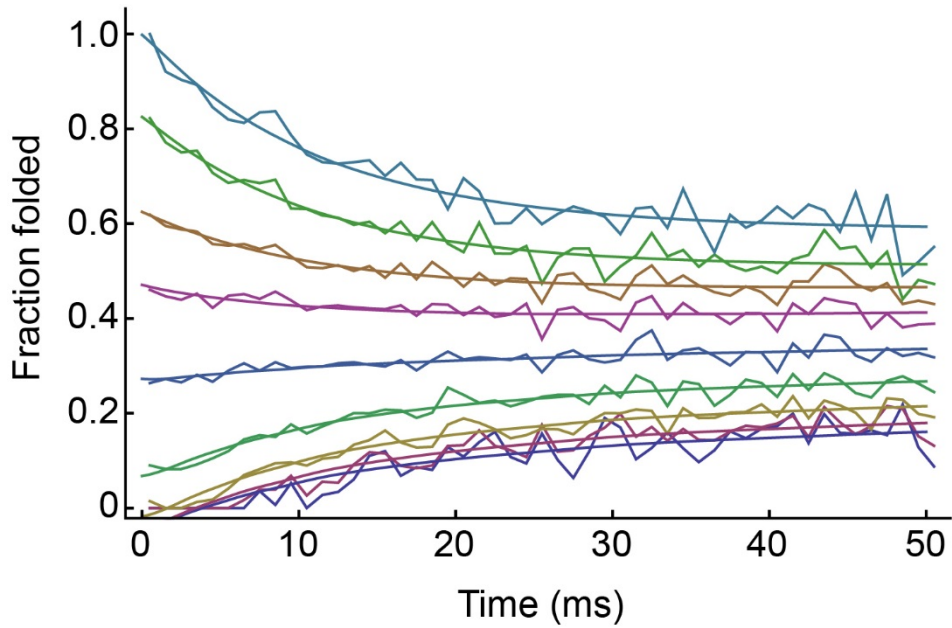
A single-molecule FRET measurement in a HeLa cell after injection of fluorescently labeled ProT $\alpha$  into the cytosol was split into two halves. The FRET efficiencies of doubly labeled ProT $\alpha$  (transfer efficiency of 0.33 to 0.35) are constant within uncertainty during the measurement in the cytosol of a single cell.



#### Supplementary Figure 14

Cellular autofluorescence makes a negligible contribution to FRET efficiency histograms in microinjected cells.

The contribution of cellular autofluorescence was investigated by performing single-molecule FRET measurements in non-injected cells. **(a,c)** Fluorescence recordings of donor (green) and acceptor emission (red) with 1-s time binning, acquired in the cytosol **(a)** and nucleus **(c)** of HeLa cells that had not been injected with fluorescently labeled protein. **(b)** FRET efficiency histograms from the measurement in the cytosol of a non-injected cell **(a)**, with different thresholds (20 – 50 photons per burst) for burst detection applied. **(d)** FRET efficiency histograms from the measurement in the nucleus of a non-injected cell **(c)**. In both cases, above a threshold of 30 (the minimum threshold used for injected cells), the number of bursts due to cellular autofluorescence is small and their contribution to the FRET efficiency histograms measured in injected cells is therefore negligible.



#### Supplementary Figure 15

Choosing different initial transfer efficiency intervals for recurrence analysis (RASP) does not affect the observed relaxation dynamics.

To illustrate that the kinetics obtained from recurrence analysis is independent of the choice of initial transfer efficiency intervals, as expected from theoretical considerations<sup>6</sup>, we calculated the fractions of folded intracellular GB1 from recurrence FRET efficiency histograms analogously to the curves shown in **Figure 4f** but with a broad range of different initial transfer efficiency intervals, from bottom to top:  $\Delta E = (0.6, 0.8)$ ,  $(0.65, 0.85)$ ,  $(0.7, 0.9)$ ,  $(0.75, 0.95)$ ,  $(0.8, 1.0)$ ,  $(0.85, 1.05)$ ,  $(0.9, 1.1)$ ,  $(0.95, 1.15)$ , and  $(1.0, 1.2)$ . All data (noisy curves) can be described with one relaxation time of 12 ms (smooth lines), the value we obtained from the analysis of the data shown in **Figure 4f**, where the intervals were  $\Delta E = (0.7, 0.9)$  and  $\Delta E = (0.95, 1.1)$ .

## Supplementary Table 1

### Amino acid sequences of prothymosin alpha (ProT $\alpha$ ), the IGG-binding domain of protein G (GB1), GB1 wildtype (GB1 wt), and the yeast frataxin homolog Yhf1.

The labeling positions are indicated in underlined boldface.

<b>ProT<math>\alpha</math></b> (S1C/E56C)	GP	1	11	21	31	41
		<u>C</u> DAAVDTSS	ITTKDLKEKK	EVVEEAENGR	DAPANGNAEN	EENGEQEADN
		51	61	71	81	91
		EVDEE <u>C</u> EEGG	EEEEEEEEGD	GEEEDGDEDE	EAESATGKRA	AEDDEDDVD
		101				
		TKKQKTDEDD				
<b>Yhf1</b> (V1M/N16C/ S120C)		1	11	21	31	41
		MESSTDGQVV	PQEVLCPL	KYHEEADDYL	DHLLDSLEEL	SEAHPCIPD
		51	61	71	81	91
		VELSHGVMTL	EIPAFGTYVI	NKQPPNKQIW	LASPLSGPNR	FDLLNGEWVS
		101				
		LRNGTKLTDI	111	121		
			LTEEVEKAIC	KSQ		
<b>GB1</b> (Q2C/F30L/ G41A/T55C)	GAM	1	11	21	31	41
		<u>G</u> CYKLILNGK	TLKGETTTEA	VDAATAEKVL	KQYANDNGVD	AEWTYDDATK
		51				
		TFTV <u>C</u>				
<b>GB1 wt</b> (Q2C/T55C)	GAM	1	11	21	31	41
		<u>G</u> CYKLILNGK	TLKGETTTEA	VDAATAEKVF	KQYANDNGVD	GEWTYDDATK
		51				
		TFTV <u>C</u>				